Oceanologia (2020) 62, 413—427

Available online at www.sciencedirect.com

ScienceDirect

journal homepage: www.journals.elsevier.com/oceanologia

ORIGINAL RESEARCH ARTICLE

Observations on relations between marine aerosol fluxes and surface-generated noise in the southern Baltic Sea

Piotr Markuszewski[a,*], **Zygmunt Klusek**[b], **Ernst D. Nilsson**[c], **Tomasz Petelski**[a]

[a] *Physical Oceanography Department, Institute of Oceanology, Polish Academy of Sciences, Sopot, Poland*
[b] *Marine Physics Department, Institute of Oceanology, Polish Academy of Sciences, Sopot, Poland*
[c] *Department of Environmental Science and Analytical Chemistry, Stockholm University, Stockholm, Sweden*

Received 8 January 2020; accepted 7 May 2020
Available online 22 May 2020

KEYWORDS
Sea spray fluxes;
Underwater ambient bubbles noise;
Baltic Sea

Summary This study presents the preliminary results of combining underwater acoustic ambient noise measurements with those of in-situ sea spray fluxes (SSF). Hydroacoustic measurements (in the frequency range 80 Hz —12.5 kHz) were made using an underwater noise recording system developed at the Institute of Oceanology of the Polish Academy of Sciences which was then deployed in the southern Baltic Sea. The simultaneous measurements of coarse sea spray fluxes (with particle diameters ranging from 0.5 to 47 μm) were made on board the r/v *Oceania* using the gradient method. Observations were conducted for the duration of the passage of an atmospheric front that lasted 2.5 days (60 hours of measurements). There were significant differences in the sound pressure level (SPL) and aerosol fluxes observed between the first part of measurements (developing wave state) and the second part (developed waves). Wave parameters, such as peak period, significant wave height, wave age, and mean wave slope acquired from the WAM (WAve Model), were used to investigate the impact of wave field properties on noise and aerosol flux measurements. We observed different behaviours in the

* Corresponding author at: Physical Oceanography Department, Institute of Oceanology, Polish Academy of Sciences, Powstańców Warszawy 55, 81—712 Sopot, Poland.
E-mail address: pmarkusz@iopan.pl (P. Markuszewski).
Peer review under the responsibility of the Institute of Oceanology of the Polish Academy of Sciences.

Production and hosting by Elsevier

https://doi.org/10.1016/j.oceano.2020.05.001

power spectrum density (PSD) levels of noise for these parameters depending on the wave state development.

1. Introduction

Despite concerted efforts within the scientific community, sea spray aerosol (SSA) is still one of the less understood and parametrised components of the earth's climatic systems (de Leeuw et al., 2011; Lewis and Schwartz, 2004; Veron, 2015). With a fairly large number of concepts and approaches notwithstanding in the effort to ascertain the relations between SSA emissions, a high level of uncertainty still hovers over those estimations. According to IPCC (2013), estimation of the amount of SSA mass transport across the planet's air-sea surface ranges from 1400 to 6800 [Tg/yr], with an uncertainty level of 80% (Tsigaridis et al., 2013). Hence, different methodologies aimed at tightening this range are to be expected.

On the one hand, the most important source of the marine aerosol is the bursting of air bubbles produced for the most part by the breaking waves (e.g. Blanchard, 1963). On the other hand, it is generally accepted as fact that the wind-driven component of underwater sea noise is mainly emitted by newly-born bubbles in the whitecapping process from wind-waves (Loewen and Melville, 1991; Medwin and Beaky, 1989). An attempt at assessing the relationship between the origin of sea surface noise at frequencies below 1 kHz and the whitecaps index has been made by Wilson (1980). Based on the historical data, he showed qualitatively similar behaviour for both quantities on wind speed. The idea of monitoring sea-salt production from the sea surface to the atmosphere by measuring the underwater noise was first put forward some years ago by Wilson and Makris (2008) but with no further development since then.

In the literature, we were able to find several attempts to correlate aerosol emission with wave parameters. The most commonly used were wave phase velocity c_p and the whitecap fraction of the sea surface (inter alia Bortkovskii and Novak, 1993; Kraan et al., 1996). Stramska and Petelski (2003) first suggested a strong correlation between sea state development and whitecap fraction which points to higher aerosol emission as well. In another study by Petelski et al. (2005) based on aerosol flux measurements and the WAM (WAve Model), sea spray aerosol flux is suggested to be proportional to the rate of energy dissipation in a wave field raised to the power of 2/3. They also observed an increasing correlation between wind friction velocity (u_*) and aerosol flux in case of increasing wave age (defined as c_p/u_*). There is a wide range of parameters which can influence aerosol emission. Another very promising parameter for future research can be the turbulent kinetic energy at the sea surface interface which was investigated by Esters et al. (2017) in terms of its relations to the Schmidt number, among others.

On the other hand, it is well recognized that at frequencies above 500—800 Hz, and in the absence of anthropogenic noise, the power spectrum of underwater natural noise shows strong wind dependence. The envelopes' spectra have the same universal shape, and do not depend on salinity; however, bubble size spectra created by wave breaking differ in terms of salt and fresh water. For sea states from 3 to 7 (Beaufort), noise spectra above 1 kHz sloped within a range of −5 to −6 dB per octave (Wenz, 1962). There is evidence that the sound pressure level (SPL) is better interrelated with the wind speed than the wind waves' energy parameters (Felizardo and Melville, 1995; Vakkayil et al., 1996). Only recently, Dragan et al. (2011) have found evidence that the wind-wave component of underwater noise could be related to the wave's age.

Finding the connections between the wind-driven noise and aerosol emission is not only thought-provoking but would also open the way to monitoring aerosol fluxes from the sea surface on the basis of underwater noise measurements. Moreover, methods for measuring underwater noise could be performed autonomously with a durable and stable setup located near the sea surface without being disturbed by weather conditions on that surface. In this paper, we propose to consider the relations between two different methods typical of their respective branch of the sciences: the SSA gradient method for atmospheric science, and underwater measurements of the bubbles' ambient noise spectrum level for physical oceanography. Besides, as is well known, the usefulness of the ambient sea noise for the monitoring of aerosol fluxes is yet to be adequately studied.

In this paper, we present the results of measurements of SSA emission compared with simultaneous underwater noise recordings. The data reported here were collected on board the r/v *Oceania* during a single pass of a cyclonic weather front over the area of the Baltic Proper.

2. Background

2.1. Aerosol generation mechanisms from bubbles

Three main classes of droplets emitted from the sea surface are usually recognized: the so-called film, jet, and spume drops. The first two are closely associated with bubble bursting processes entrained to the water when the wind wave is collapsing. Film drops are emitted from the bursting of a thin bubble coat, while jet drops are injected into the air by the bubbles' cavitation, and spume drops are torn from the whitecaps' crests under strong wind conditions. All mentioned processes were originally described by Andreas (1995), Blanchard and Syzdek (1988), MacIntyre (1972), Resch et al. (1986), among others.

Using fast and precise photos of bursting bubbles (Lhuissier and Villermaux, 2012; Spiel, 1998), it was found that the size of film drops ranges from 20 nm (Sellegri et al., 2006) to hundreds of microns (Afeti and Resch, 1990). Most of these droplets are less than 1 μm. Film droplets are responsible for the transport of oceanic surface matter to the atmosphere (Blanchard, 1964).

Jet drops are emitted during the collapse of a bubble's cavern. They are injected as a narrow water stream with high acceleration. The size spectrum of such droplets is highly dependent on the parent bubble's size. It is estimated that droplet sizes are 0.13–0.15 times smaller than the bubble size (Wu, 2002). The size spectrum of such droplets covers a range of 1 μm $< r_p <$ 50 μm, with a maximum at 10 μm (Lewis and Schwartz, 2004).

The process of spume drops torn from the waves crests was first investigated by Koga (1981). Emission starts when the wind speed is higher than 7 m/s. The size range of particles emitted via this mechanism is estimated to be radii 10–500 μm, with a peak at 100 μm (Andreas, 1998, 1992; Andreas et al., 2010; Fairall et al., 1994; Smith et al., 1993; Wu, 1981, 1993).

Another emission process is indissociably linked with splash drops (Andreas, 1998). This kind of droplets is less important for emission and its observation relatively difficult. Wind waves collapsing during breaking hit the sea surface and can saltate as splash drop to air (Kiger and Duncan, 2012). Splash and spume drops' emission can depend on the wind or waves but the intensity of aerosol emission can also be fortified by rainfall (Marks, 1990).

2.2. Sea spray generation function for the Baltic Sea

The most reliable of the direct techniques for determining the marine aerosol fluxes are micrometeorological methods. Through the micrometeorology approach, fluxes of the effective SSA production are deduced from direct measurements of the fluctuation or gradient of SSA concentration in the near-water boundary layer (constant fluxes assumption). The most important techniques in this approach are the eddy covariance method (EC) and gradient method (GM).

The GM approach was first proposed by Petelski (2003). The first flux parameterisation, based on aerosol gradient measurements in the northern Atlantic Ocean using GM, was provided by Petelski and Piskozub (2006) and later modified by Andreas (2007). In the more recent literature, the usability of the GM method was confirmed repeatedly by Savelyev et al. (2014) on board the Floating Instrument Platform (FLIP) in the Pacific Ocean or on board the r/v *Oceania* in the southern Baltic Sea region (Markuszewski et al., 2017a; Petelski et al., 2014).

In order to make a parameterisation of the sea spray emission, the so-called sea spray generation function (SSGF) was used. A thorough review of the proposed SSGFs has been conducted by de Leeuw et al. (2011). All known parameterisations are highly scattered on account of the different approaches, parameters, and methodologies used.

The direct relation between aerosol flux, wind speed, and aerosol size with respect to the Baltic Sea area was given by Petelski et al. (2014) in the form of:

$$F_{p14}(U_{10}, D_p) = (1.83 \cdot 10^4 \cdot U_{10}^2 - 1.35 \cdot 10^4) \exp(-0.62 \cdot D_p), \quad (1)$$

where F_{p14} is SSGF as given by Petelski (2014), U_{10} is the wind speed at a height of 10 m above the sea surface, and D_p is the particle diameter with a particle range of 0.5 μm to 8 μm.

Another model of sea spray emission was proposed by Massel (2007). Based on dimensional analysis and deep theoretical considerations, he combined sea spray emission with wave state properties using two approaches. The first approach is the limiting steepness (LS) criterion:

$$F_{ls}(H_s, \omega_p, D_p) = F_{prod}(D_p)\left[-0.1933 a_0 \left(H_s \cdot \frac{\omega_p^2}{g}\right)^{-2}\right]. \quad (2)$$

The second is threshold vertical acceleration (TVA):

$$F_{tva}(H_s, \omega_p, D_p) = F_{prod}(D_p)\left\{1 - \Phi\left[0.447\left(H_s \cdot \frac{\omega_p^2}{g}\right)^{-1}\right]\right\}, \quad (3)$$

where, F_{ls}, F_{tva} are defined as the size-dependent SSGF, $F_{prod}(D_p)$ is a single whitecap spray emission, a_0 is the constant of spectral moment equalling 0.3048 (Massel, 2007, appendix D), Φ is the probability integral (Abramowitz and Stegun, 1975), and g is the gravitational acceleration. The peak frequency ω_p may be determined from the peak period: $\omega_p = 2\pi / T_p$.

The whitecap spray emission F_{prod} was assumed as Woolf's function (Woolf et al. 1988) determined from the Monahan model (Monahan et al. 1986), which can be formulated as follows:

$$F_{prod}(D_p) = \exp\left[16.1 - 3.43\log\left(\frac{D_p}{2}\right) - 2.49\log^2\left(\frac{D_p}{2}\right) + 1.2\log^3\left(\frac{D_p}{2}\right)\right]. \quad (4)$$

In order to obtain the total aerosol emission, all functions were integrated by the size distribution within the range D_p=(0.5 − 47 μm).

The majority of SSGFs are determined on the basis of measurements in the open ocean area. Due to the fact that the Baltic Sea is an inland-type sea with brackish water, the spectral properties of the wind-waves and mass fluxes may be different from those of the open ocean. A most pertinent comparison between sea spray flux measurements and several SSGFs (Callaghan, 2013; Massel, 2007; Petelski et al., 2014) has been provided by Markuszewski et al. (2017a).

However, the key question that remains is how to deal with the problem of the enormous spread of source function values as in the literature (some orders) and a more precise identification of the aerosols' sources, which could provide a guideline towards achieving a desirable outcome.

2.3. Noise-wind relationships

Underwater noise that is measured near the sea surface provides universal and, in principle, an ever flow of information

about dynamic processes such as wind speed, wave energy dissipation, and rain rate (Felizardo et al., 1995; Nystuen, 2001; Vagle et al., 1990; Zedel et al., 1999). These results from previous experiments have shown that the ambient noise generated at the sea surface was better parametrised by the local wind speed but not so well correlated with the height of the wind wave.

In many of the world's oceans as well as in the Baltic Sea (Klusek and Lisimenka, 2016), it was established that underwater noise in the wind-dependent frequency range, i.e. approximately above 1 kHz, shows a near-quadratic dependency with wind velocity. Consequently, underwater noise anemometers (for wind speed and air-sea fluxes estimation) were proposed and put into practice (Zedel et al., 1999, SWADE anemometer). The objective of this work is to establish the degree of dependency between SPL and aerosol fluxes for the possible implementation of monitoring by way of the more difficult-to-accomplish measurable process of aerosol production using simply measured ambient sea noise from the sea surface.

Our proposal is based on well-established facts: breaking waves entrain air bubbles under the sea surface which are the sources of underwater noise. When these bubbles return to the sea surface and burst, they emit a number of tiny droplets. Thus, both processes are contingent upon the bubble rate production so that there should be a functional relation between the investigated parameters.

In the same way, as in the source functions for aerosols, it is generally accepted that the intensity of ambient sea noise from natural sources has a broad frequency range. In particular, a strong dependency on wind ranges from some hundreds of Hz (400–800 Hz) all the way to tens of kilohertz, where wind speed above 3–4 m/s and less than 14–16 m/s grows as a power function of the wind speed (Crouch and Burt, 1972):

$$p^2(f \pm df) \propto u_{10}^{n(f)}, \tag{5}$$

where $p(f)$ is the acoustic pressure around frequency f in frequency band $f \pm df$, while the exponent of this relation $n(f)$ depends on the frequency.

Given the presence of anthropogenic sources (mainly nearby ships and traffic noise) for a relatively short time series of observations, determining the wind-dependent factor $n(f)$ in the Baltic Sea is not so simple a task. This is due to difficulties in separating and eliminating signals in which the level of noise generated by passing ships is comparable to the noise from natural sources.

2.4. Underwater noise generation

The contribution of natural noise created by bubbles in the first phase of their formation is considered a major input to sea noise with a broad frequency range. However, different variations in bubble shape are responsible for sound emission, with the main mechanism being the radial oscillation of bubbles wherein the size of the bubble determines the frequency of the emitted sound. The classical Minnaert formula (Minnaert, 1933) for the resonance frequency of gas bubbles in the fluid when the surface tension forces would be neglected is given in the form:

$$f_0 = \frac{1}{2\pi\sqrt{r_b}}\sqrt{\frac{3\gamma p_h}{\rho}}, \tag{6}$$

where, r_b is the bubble radius, ρ is the water density, p_h is the hydrostatic pressure, and γ is the heat capacity ratio.

At lower frequencies in a range of up to several hundreds of Hz, the noise originating from bubble clouds oscillates as a whole, and above 1 kHz at up to tens or even hundreds of kHz from the oscillation of single bubbles mainly at their resonance frequency. Theoretical explanations and estimates of noise from different mechanisms have been established in a couple of studies, both theoretical and experimental (Kerman, 1984; Medwin and Beaky, 1989; Prosperetti et al., 1993; Prosperetti, 1988). The bubbles' size distribution is determined by two main mechanisms. Smaller bubbles (smaller than 1 mm) are created by jet drop impact at the wind waves while the bubbles' density is proportional to the power factor −3/2 of bubble radius. Bigger bubbles are driven by turbulent fragmentation and can be described as the power factor −10/3 of bubble radius (Deane and Stokes, 2002). Thus, the spectrum of noise emitted by mechanically excited single bubbles reflects bubble size spectra, range of radii in a bubble population, and the size of bubble clouds.

3. Materials

3.1. Measurements sites

The most representative and least contaminated areas for estimating marine aerosol fluxes are the central basins of the sea. From an acoustic point of view, underwater sea noise in the Baltic Sea is highly contaminated due to the input of sounds from anthropogenic sources, mainly the high-intensity noise of marine traffic. Underwater ambient noise from wind-driven sources could be considered 'normal' or 'typical' for a given area where the influence of ship noise is observed to be minimal. Furthermore, the choice of the point of observation depends to some degree on the wind direction, research vessel's time, and the ability to recover the submersible acoustic buoy after observations in a manner that is safe. In particular, aerosol measurements must fulfil the stricter requirements of quality rather than the ones from noise. This is because it is easier to make a selection of the noise data time series during reprocessing to remove contamination by ship noise.

The data collection is carried out at a site located in the vicinity of the Słupsk Bank (55°31′N, 17°18′E). The analysed data were retrieved from deployments of the IO PAN acoustic buoy system between 21–24 October 2015. The ship was anchored at 1 NM east of the buoy's position. This distance was previously tested and found satisfactory save the uncontaminated measurements of noise from natural sources.

4. Methods

4.1. Meteorological conditions

The main measurements were conducted during 22–23 October 2015. On October 22, the region of measurements

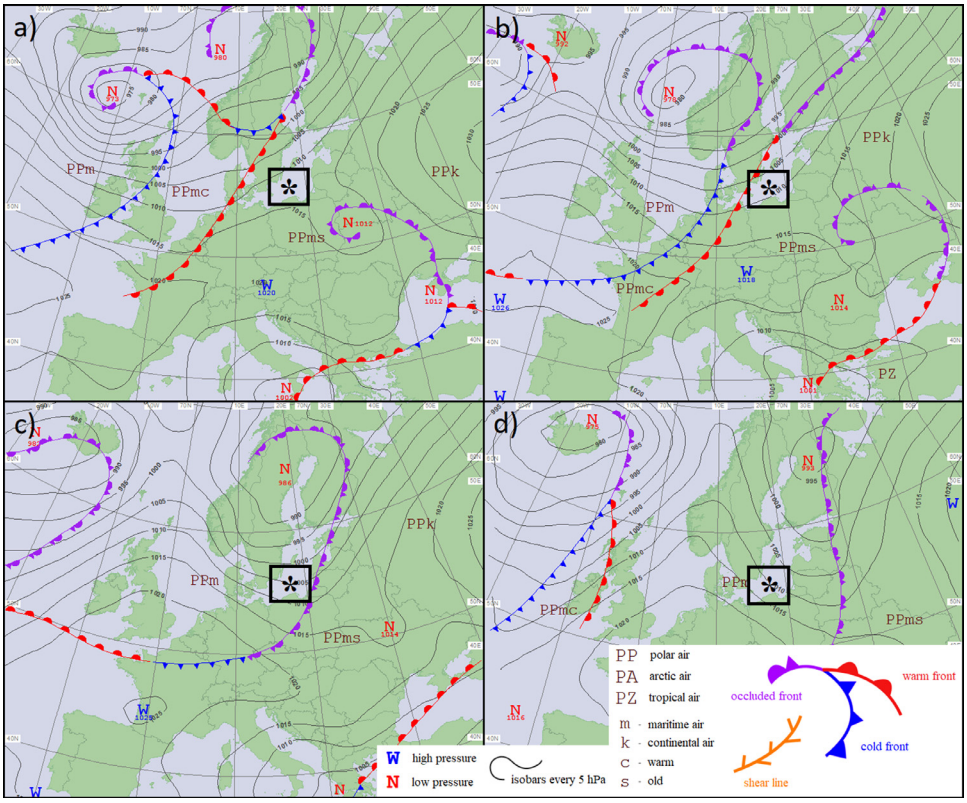

Figure 1 Synoptic charts: (a) 00 UTC on the 22nd, (b) 12 UTC on the 22nd, (c) 00 UTC on the 23rd, and (d) 12 UTC on the 23rd October. The asterisk shows the location of the measurement area (55°31′N, 17°18′E). Charts were prepared in IMGW-PIB, CBPM in Kraków (http://www.pogodynka.pl/polska/mapa_synoptyczna).

was under the influence of a weakening low-pressure system from Belarus (Figure 1a). The deep low-pressure area from Faroe Islands (973 hPa) determined the air mass oscillation in the region of measurements during the days of measurement that followed. From the west of the Baltic Sea, warm and cold fronts were approaching (Figure 1a–b) towards the ship's position. As a result, in the middle of the measurements, an occlusion front occurred. During the passage of this occlusion, there was only minor rainfall (up to 2 mm/h) observed. For the duration of the rainfall, the results of aerosol flux measurements were rejected.

During the second day of observations (Figure 1c–d), the low-pressure system moved eastward and into Scandinavia. At the same time, the occlusion front passed over the Baltic Sea. These dynamic synoptic situations determined the fresh polar-marine air masses in the measurement area.

The results of aerosol gradient flux measurements were divided into two parts, i.e. before and after the passage of the front. For safety reasons (the weather forecast predicted high winds and waves), measurements were halted just after the front had passed.

4.2. Wave and atmospheric data source

Wave parameters (wave peak period T_p, significant wave height H_s) used in this work were retrieved from the Baltic Bottom Base (BBB) database developed by the Maritime Institute in Gdańsk. The database offers a wide spectrum of parameters calculated using the third generation WAve ocean Model (WAM). The detailed physics of the model is provided in the literature (WAMDI Group 1988; Hasselmann et al., 1973; Komen, 1994). The wind data in the WAM model is taken from the Mesoscale Prediction Model COAMPS (Coupled Ocean/ Atmosphere Mesoscale Prediction System), which was provided by the Interdisciplinary Centre for Mathematical and Computational Modelling in Warsaw. Its application, discussion and comparison with measurements of such databases have been presented by Markuszewski et al. (2017a). The temporal resolution of the available data was 1 hour. The spatial resolution was 1 nm (~1.85 km).

The acoustic anemometer (OMC-118 Ultrasonic Wind Sensor of the Observator Instruments) used in measurements was placed on the bow of the ship at 10 m above the sea surface. An average of over 10-minute values of wind speed was used for further analysis. The maximum value of measured wind speed was 14.9 m/s with gusts of up to 17.5 m/s. The minimum value of the wind speed was 6 m/s. The measured air temperature and pressure during measurements oscillated from 10.2°C to 12.4°C and from 1003.9 hPa to 1017.4 hPa, respectively.

4.3. Aerosol measurements

Measurements of the sea spray concentration were taken using the classical aerosol spectrometer CSASP-100-HV of the Particle Measuring Systems. This device allows for measuring the aerosol size distribution in the range D_p=(0.5 μm, 47 μm). This type of spectrometers was widely used in many

campaigns (de Leeuw et al., 2000; Hoppel et al., 1994; Jensen et al., 2001; Markuszewski et al., 2017b; Petelski, 2005). In order to eliminate the impact of humidity on the sizes of particles, all gathered aerosol data were reduced to 80% of the relative humidity wet radius using the formula provided by Petelski (2005).

4.3.1. Gradient aerosol fluxes

To determine the aerosol flux, the gradient method was used (Petelski, 2003). According to the Monin-Obukhov theory (Monin and Obukhov, 1954), particle concentration can be considered a scalar property of the air. On that basis, we can thus define the scale of particle concentration as:

$$N_* = \frac{F_N}{u_*}, \tag{7}$$

where F_N is the aerosol flux.

In order to determine N_*, the atmospheric surface layer over the sea for the aerosol composition can be expressed as a logarithmic function of specific height z:

$$N(z) = N_* \ln(z) + C, \tag{8}$$

where C is an integration constant, and N_* is determined based on aerosol concentration measurements on five altitudes (from 8 m to 20 m above sea level). In that way, we can calculate the gradient of aerosol flux from Eq. (7). The detector was mounted in a special lift which allowed for moving it between these altitudes. The measurement at each level lasted at least 2 minutes. The overall averaging time for one aerosol flux estimation was 30 minutes. Based on the measurement channels of the aerosol spectrometer, there were partial fluxes calculated using the gradient method as well.

The gradient method used in obtaining aerosol fluxes was successfully used during several campaigns in different marine regions such as the northern Atlantic Ocean (Petelski, 2003, 2005; Petelski and Piskozub, 2006), Baltic Sea (Petelski et al., 2014), and the northern Pacific (Savelyev et al., 2014). The advantages of this method include a simple design set and the low cost of measurements (no need for fast particle counters in contrast to the eddy covariance method).

4.3.2. Error propagation of aerosol measurements

The absolute uncertainty over the particle counter can be obtained from Poisson's distribution properties which denote the standard deviation $\sigma_p = \sqrt{\mu}$, where μ is the average number of counts after multiple repetitions of measurement. Based on that fact, the relative uncertainty can be defined as $(\mu^{1/2}/\mu)^*100\%$, hence inversely proportional to the average number of counts. As such, for counts in the range $\mu \sim 10^3$, $1/(m^2 s)$ (what was typical for particle size ranging from 0.5 to 2.5 μm), the relative uncertainty is $\Delta\mu \sim 10\%$. For $\mu \sim 10^3$, $1/(m^2 s)$ (in particle size ranging from 2.5 to 7 μm), $\Delta\mu$ rises to as much as 31%. For particles, a bigger particle uncertainty has a range of 90%.

4.4. Acoustic methods

4.4.1. Setup

The acoustic setup used in the experiments is the one manufactured in the IO PAN acoustic recording systems, based on an ADC (Analog to Digital Converter) microprocessor and characterized by a low self-noise level and low power consumption. The photo of the device just before deployment along with a schematic presentation of the underwater orientation is presented in Figure 2.

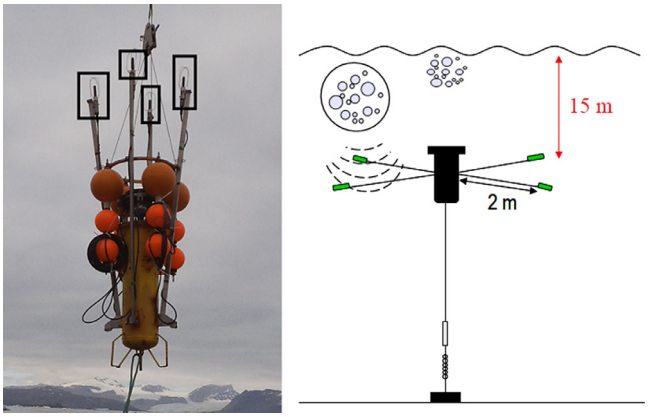

Figure 2 The acoustic recording system with four hydrophones (left panel) and its schematic underwater diagram (right panel).

The buoy is equipped with four omnidirectional Reson TC 4032-5 hydrophones placed horizontally and attached at the ends of perpendicularly distributed poles. The distances from the hydrophones to the vertically oriented cylindrical container with electronic and power supplying batteries amounted to 2 meters. So, the opposite hydrophones were at a distance of 4.4 m. Hydrophones were deployed at a depth of 15 m below the mean sea surface (the depth of deployment is measured by a pressure recorder). The deployment depth chosen was sufficiently deep so as to avoid dynamic disturbances from surface waves and yet appropriately shallow to be able to listen to single breakers. The buoy was anchored at a depth of about 40 m with sandy sediments in the area. When taking the compass sensor or inclinometer readings, we did not observe any jerks, rapid system tilts or turning.

The main task of the measuring system is to register wind or rain components of underwater noise. To avoid overdriving of preamplifiers by strong signals from marine traffic noise, the bandwidth of the tract was reduced to a frequency range of 80 Hz to 12.5 kHz. The recordings were performed with a sampling frequency of 30 kHz in each channel, in a 16-bit dynamics range. Raw data were acquired in periods of 20-second recordings with a 30-second pause.

4.5. Acoustics data analysis

The signals' recorded time series were analysed offline in a laboratory. The post-processing and statistics were performed in the MATLAB environment. Voltage was recalculated to the acoustic pressure according to the hydrophone manufacturer's sensitivity specifications. The narrow band spectra were computed from 16,384-size subsamples using the FFT (Fast Fourier Transformation) procedures, first averaging over time in 20-sec intervals and then after averaging in one-third octave frequency bands. The power spectrum density (PSD) levels of noise in each one-third octave band

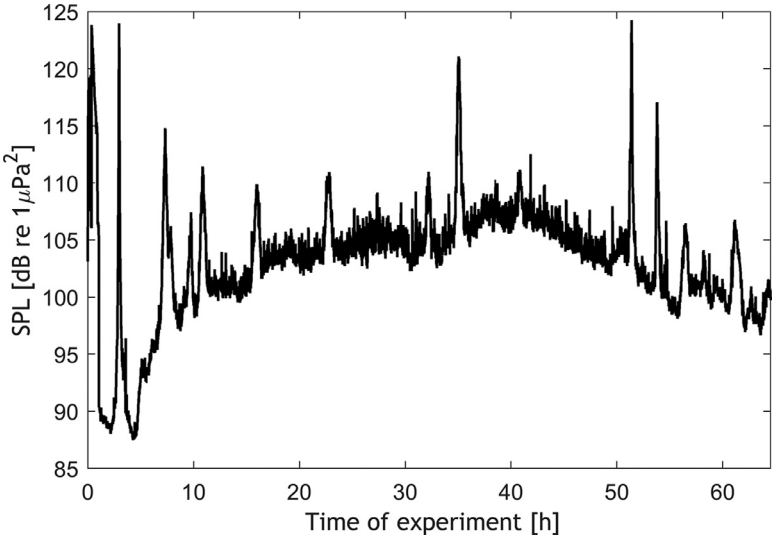

Figure 3 History of sound pressure level (SPL) observed in the entire frequency range (80 Hz–10,000 Hz) collected in subsequent 20-sec. recordings. The *x*-axis shows the time of experiment, in hours, counted from the moment of the buoy's deployment on 21 October 2015, at 14:00.

(dB re 1 μPa^2/Hz) were used as the measure of the underwater sound due to its simplicity and general use in acoustics.

Besides wind sources, commercial shipping and ferry traffic are found to be significant, however intermittent they might have been as contributors to underwater SPLs in the deployment area. The automatic algorithms aimed at the vessels' noise detection with a substantial addition to natural noise are either indefinite or time-consuming. The spectra parameters used as measures of similarity to distinguish the noise emitted by natural sources from that of ships were the centre of gravity of the individual spectra, slope of spectrum level at frequencies above 630 Hz, and most useful SPL in the whole frequency range. The last one presented in Figure 3 (as the SPL in dB re 1μPa^2) is calculated by integrating the pressure spectral density curve in narrow bands over the whole recorded frequency bands.

The time history of the broadband SPL in the analysed frequency range (i.e. between 80 and 12,500 Hz) recorded at the Słupsk Bank and extended over 60 hours is given in Figure 3. Measurements started at 14:00 21 October 2015. From the behaviour of the SPL time series, the evidence of a minimum of 14 passing ships is conspicuous, as indicated in Figure 3.

The noise data was transformed from an internal format recorded by the ADC system to the WAV (wave form audio) format to confirm the type of source via sound checking. Listening by an operator, together with further numerical processing, allows for detecting and verifying the presence of fragments of anthropogenic pollution of noise from natural sources at the sea surface.

The most important effects of the ship's noise on the form of spectra are the appearance of narrow peaks in the high-resolution spectra and relatively quick-rising SPL in the broadband range (the SPL and rate of its variation are determined by many factors such as the course of the ship in relation to the buoy, the nearest range at which the ship had passed the anchored buoy, the class of ship, sound propagation conditions, etc.). Recordings in which noise was recognised as having been emitted from ships passing by had been removed from further analysis with a simple algorithm whose design is based on the background SPL having been exceeded (Figure 4).

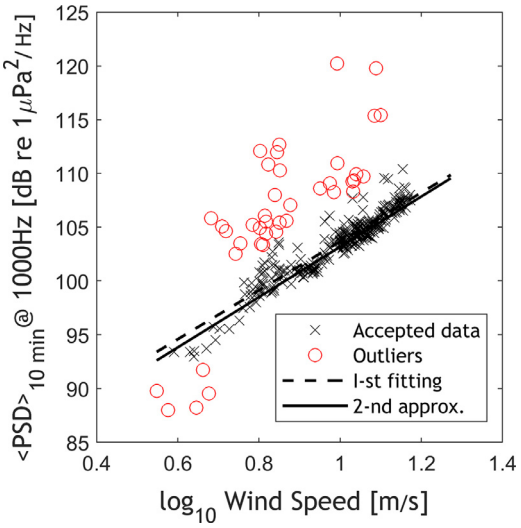

Figure 4 The example presenting the outlier removal algorithm, in which the vessel's noise exceeds the noise from natural sources. The dashed (upper) line depicts the best-fit approximation to a complete set of data. Red circles represent the data at a distance of 3 dB from the best fit line, which were removed. The process of fitting was repeated. (For the interpretation of references to colours, the reader is referred to the web version of this article.)

The principle of the exclusion algorithm of recordings when the ship's noise prevails over the noise from natural sources is presented, as an example, in Figure 4. Data are averaged in 10 minutes PSD in a one-third octave band with a central frequency of 1 kHz, i.e. the frequency band where the best correlation with the wind is observed. At the first

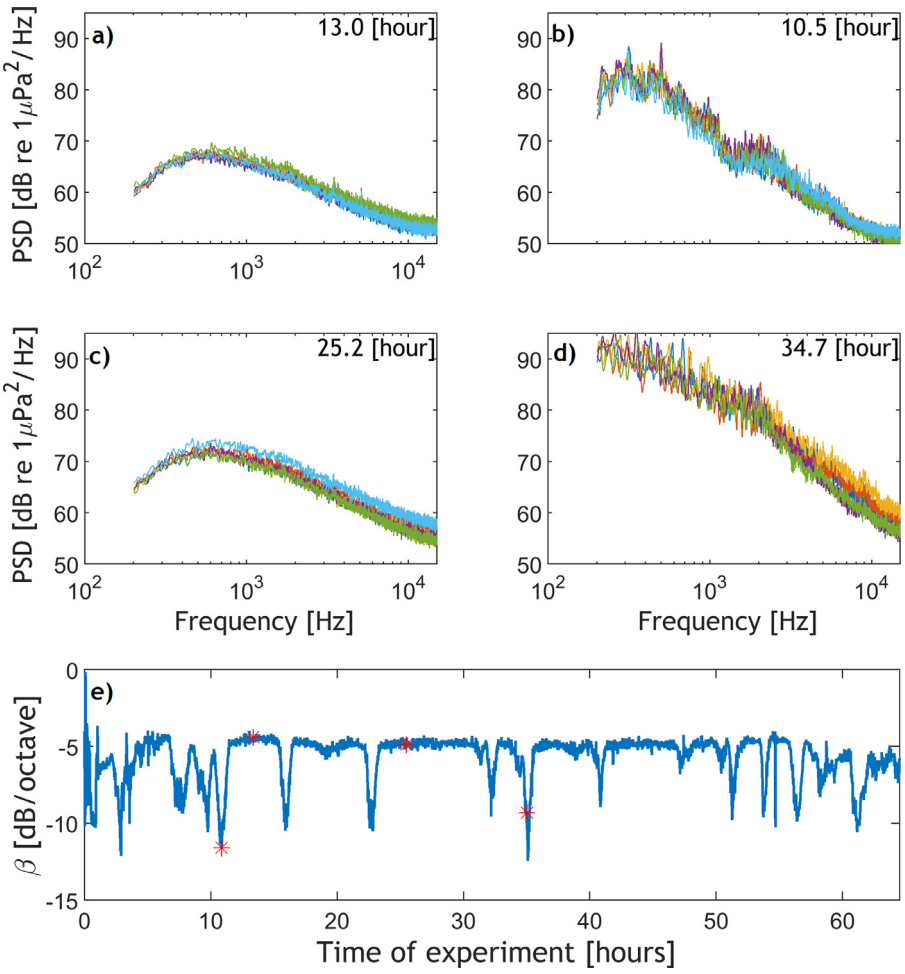

Figure 5 Examples of underwater noise spectra with no noise from ships (left panels (a) and (c)), and with a significant contribution from the shipborne component (two right panels (b) and (d)). The numbers in the upper right corner represent the position of the examples on the time axis. Time series of spectral slopes β of PSD for records collected in consecutive one-minute intervals is presented on panel e), where the asterisks indicate corresponding examples from the upper panels.

step, a best-fit approximation of Eq. (5) to an entire set of data was applied (dashed line). Using this initial guess regarding the fitting parameters, the data at a distance exceeding 3dB above the fitted curve (labelled with red open circles) had been classified as the ship's noise which was afterward removed from the database before the process of fitting was repeated. Moreover, outliers at 3dB below the first step fit line were eliminated. The presented data refer to wind speeds exceeding 3.5 m/s, i.e. when the first surface waves break.

The characteristic results of spectral analysis for records representing natural noise and with a significant contribution from ships are shown in Figure 5. Each panel a–d contains five consecutive spectra (averaged over 1 minute). The numbers in the upper right corner represent the position of examples on the noise recording timeline. Depending on the type of the noise's prevailing component, not only the sound level but also the slope of the spectrum is modified. For noise from natural surface sources at frequencies exceeding several hundred Hz, it is about a −5 dB/octave. Whereas in the presence of noise from a ship when the ship is far enough from the observation point, we can observe two ranges with different slopes of the spectrum envelope, contrary to a practically constant slope when the ship is close. In addition, in a fairly continuous and smooth noise spectrum, peaks from the ship's machinery and propeller appear. Spectral slopes β for each 1-minute record are given in Figure 5e, where asterisks represent examples from Figure 5a–d.

After removing data contaminations from the shipping noise, the final parameters of ambient noise versus wind relationships are calculated, while associations concerning underwater SPLs, wind speed, aerosol fluxes and wave parameters are analysed using the ancillary datasets.

The data were used to determine the coefficients $n(f)$ of the noise's wind dependence in different frequency bands for situations where $u_{10} > 5$ m/s when the first whitecap appears. The results of computing the values of exponent $n(f)$ in each of the 1/3-rd octave frequency bands are presented in Figure 6, wherein the x-axis is the frequency.

We notice the proximate quadratic functional dependence of the noise intensity on wind speed for frequencies above 630 Hz during the period of observation. The largest values of the set of $n(f)$ coefficients and the strongest cor-

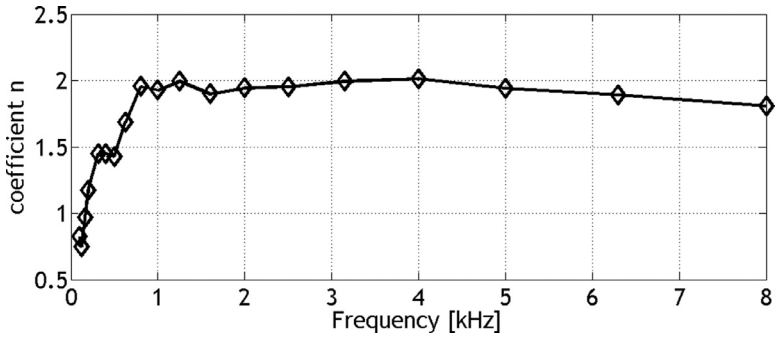

Figure 6 Values of the wind speed dependency factor $n(f)$, (Eq. (5)) in each analysed 1/3-rd octave band.

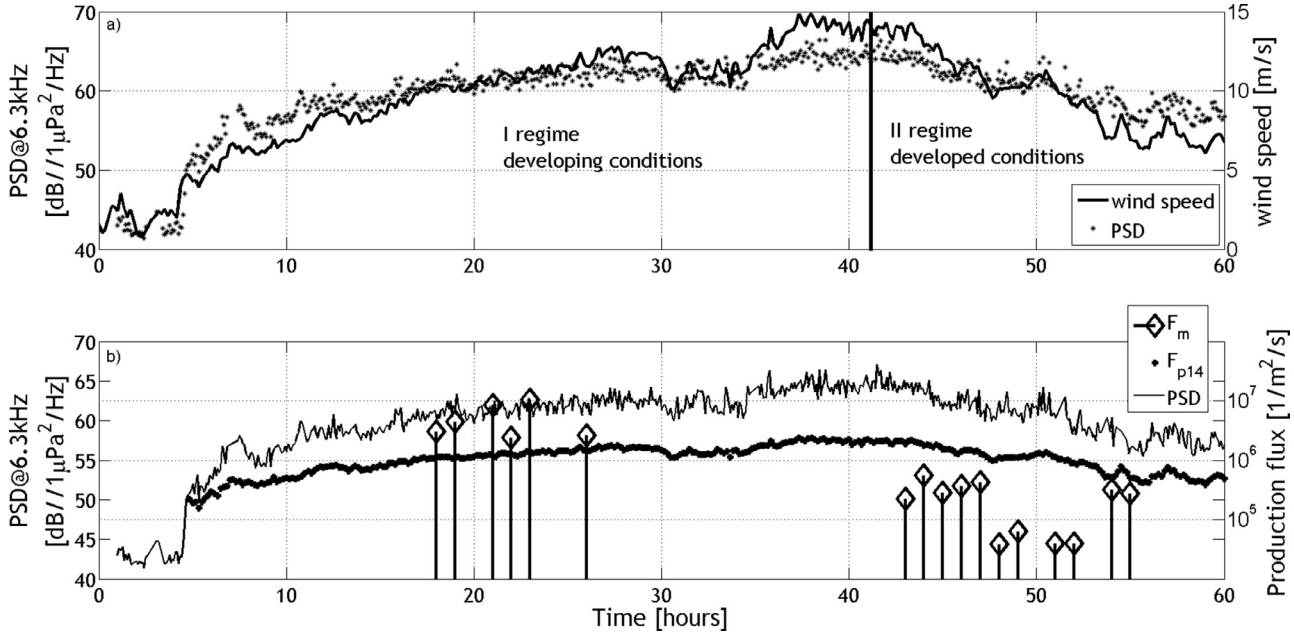

Figure 7 Concurrent time series of the Power Spectral Density of underwater noise at 6.3 kHz (PSD@6.3 kHz) and wind speed (upper panel); with PSD as the measured total aerosol gradient flux F_m and calculated fluxes based on Eq. 1 and integrated for particles' diameters ranging from 0.5 μm to 47 μm (lower panel). The *x*-axis shows the time of noise measurements from the start. The vertical line on the upper panel demarcates developing wind wave conditions from developed ones.

relation of noise intensity with the wind are observed in the bands between 1000 and 4000 Hz. In a lower frequency range, the noise is less dependent on the local wind speed due in part to the profound influence/input of distant noise sources on the recorded data.

The derived associations between the noise spectral density level from wind-dependent sources and wind speed seem akin to the noise-wind relations presented earlier (Klusek, 2011; Klusek and Lisimenka, 2016) in the same frequency range, with the wind speed of up to 14 m/s and for acoustic frequencies at up to 12.5 kHz. With increasing frequency, the $n(f)$ values become fixed and diminish only slightly when approaching 10 kHz.

The steadily observed trend of diminishing n value with increasing frequency is insignificant, and might be explained by the rising frequency losses in sound intensity coming from more distant sources. Thus, the use of noise in a broad frequency band as the indicator of bubble production and aerosol emission seems reasonable.

5. Results and discussion

5.1. Interconnection of noise—aerosol fluxes

A concurrent time series of the underwater SPL's power spectral density level in the 1/3-rd octave at a central frequency of 6.3 kHz, together with the wind speed, is shown in the upper panel of Figure 7, while the PSDs combined with the measured aerosol fluxes and SSGF approximation (Eq. (1)) are presented in the lower panel of Figure 7.

The noise data are given over 5-minute periods as average after removing recordings when the ship's noise makes a significant contribution to the recorded noise. The noise data are used for a relatively high-frequency band such as 6.3 kHz for the reason that at higher frequencies, the background ship component of underwater ambient noise makes smaller contributions to the summary acoustic field. The

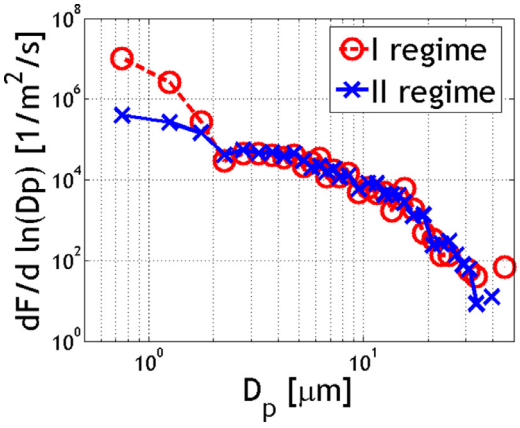

Figure 8 The averaged size distribution of particle fluxes in two emission regimes. I regime: before passing of the front, developing wave phase, wind rising up; II regime: conditions after the front, wave phase developed, decreasing wind condition. (For the interpretation of references to colour in this figure legend, the reader is referred to the web version of this article.)

correlation between measured wind speed and PSD at 6.3 kHz was high (R=0.97).

Aerosol data measurements have been conducted in the two regimes related to wave state development. The first subset was collected during the growing wind phase, while the second was performed after the occlusion front had passed. There are quite different conditions for the generation of bubbles, with the consequence for both noise and sea spray aerosols. During the first period of measurements, the wave age was below 1, while the mean wave slope was higher than a value of 0.03. In the second regime of measurements, the wave age started to increase, while the mean wave slope decreased below the 0.03 value (Figure 9b). The transition between regimes started changing after the 41st hour of measurements.

The atmospheric conditions allowed for calculating only the mean values of partial fluxes in 36 size bins (subsection 4.1.1) for both regimes of wave field development. In Figure 8, we can see the difference in the SSF size distribution. For the smaller particle diameters (D_p<2.25 μm), in the first observation regime, the aerosol flux was higher than that for the second regime. For bigger particles, the observed emission was similar.

Additionally, when wind speeds exceed 9 m/s, spume drops are produced by being torn from the wave crests (Monahan et al., 1983), part of which ascends into the air while the other part lands on the sea surface. It would be expected that spume drops striking the water surface would emit noise during the hydraulic jump or cause additional bubble generation. Nevertheless, we do not observe any growth in the SPL when wind exceeds this threshold. It indicates that the main source of noise is bubbles generated during wave breaking. It is obvious that variations in time series (presented as logarithmic quantities) almost overlap each other.

5.2. Noise — interconnections of wave parameters

There are two important parameters that inform the stage of wave field development. One is wave age which is a dimensionless parameter defined as the ratio between wave phase velocity and wind speed: c_p/U (Massel, 2018). The wave phase is determined on account of the wave peak period according to the formula: $c_p=gT_p/(2\pi)$. The other parameter that informs the development of a wave state is the mean wave slope defined as: $sl=2\pi H_s/(gT_p^2)$. We assumed that values sl>0.03 represent an undeveloped wave state, while lower values correspond to developed waves (after Bourassa et al., 2001).

Wave parameters, such as the peak period T_p and significant wave height H_s during measurements, are presented in Figure 9 (upper panel). In the analysed time series, the peak period and significant wave height increased along with the wind speed. The transition between regimes occurred when the mean slope started to decrease near the boundary value of 0.03, as shown in Figure 9 (lower panel).

Because the temporal resolution of the modelled parameters was 1 hour, the PSD values were averaged to the same resolution, with the results of the comparison shown in Figure 10. We can observe certain differences between both selected wind regimes. In the period with increasing wind conditions, significantly higher values of PSD were observed than for the period with decreasing wind conditions (Figure 10, upper panel).

5.3. Noise — comparison of sea spray models

In Figure 11, the total measured aerosol fluxes were compared with the theoretical values obtained using three different generation functions. The first was the typical experimental function and wind speed-dependent F_{p14} (obtained from Eq. (1)), while the other two were wave properties that depended only on two different wave regimes (F_{ls} — Eq. (2) and F_{tva} — Eq. (3)).

As can be seen in Figure 11a, in the first stage of measurements the regime of limiting steepness best describes the total aerosol flux. In the second stage, the function determined on the basis of wave regime and defined as the threshold vertical acceleration best predicts the aerosol emission. The last two outlier points (54 and 55 hours of measurement) can be explained as the result of unsteady dynamical wind-wave conditions. It could have been caused by local wind gusts which can be observed in several uprising episodes of PSD and wind speed between 50 and 60 hours of measurements (Figure 7). Such dynamical gusts provided additional input to the turbulence energy and thus increased the aerosol emission in this period.

The wind speed-dependent function F_{p14} was determined based on several field campaigns in different atmospheric and wave conditions (Petelski et al., 2014), so it can be treated as the average value of the measured fluxes. As can be seen in Figure 11, in the first stage of measurements, the fluxes were higher than those predicted by this function. In the case of the developed wave state, the measured fluxes were lower than the theoretical values. Similar results were also observed by Norris et al. (2012) when applying the eddy covariance method.

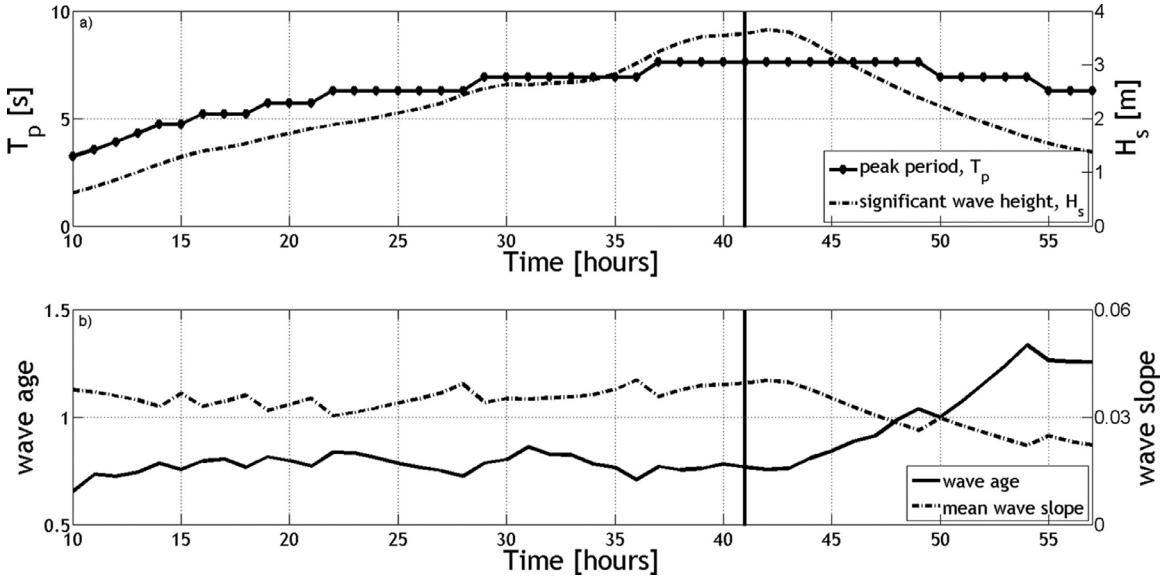

Figure 9 The upper panel shows a time series of wave parameters obtained from the Baltic Bottom Base (BBB) calculated using the WAM3 model. In the lower panel, the calculated dimensionless numbers describing the properties of wave development are shown.

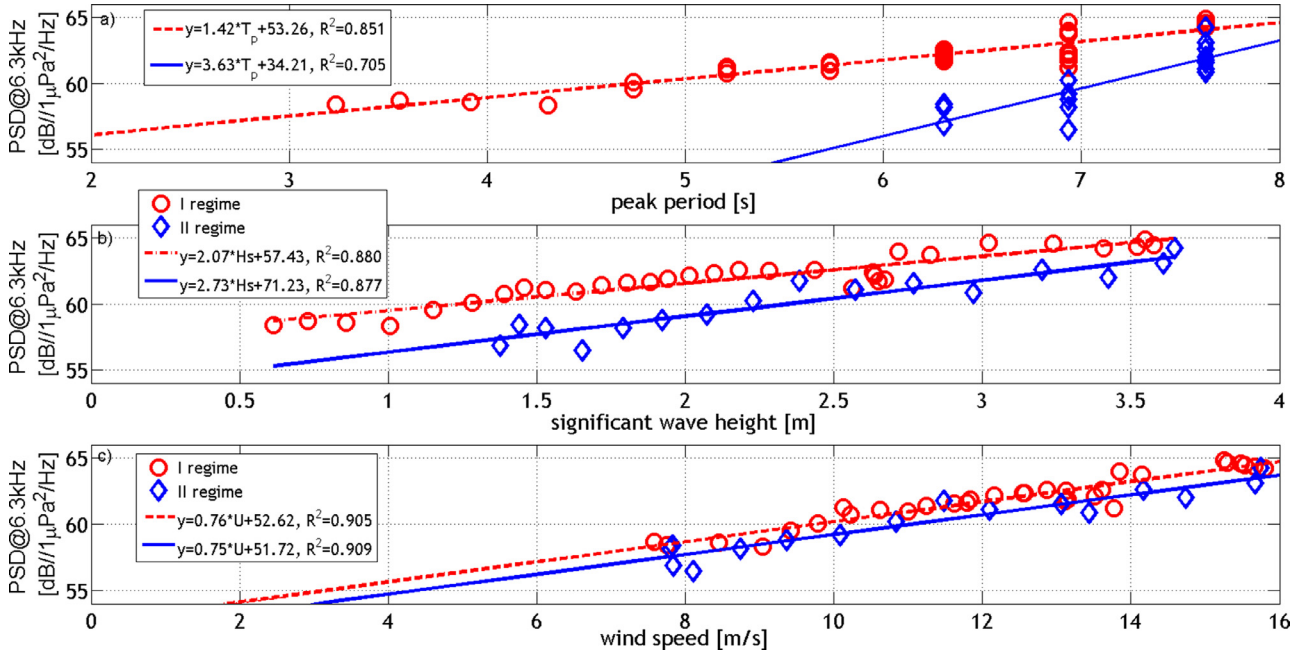

Figure 10 Comparison of 1-hour averaged Power Spectral Density at 6.3 kHz (PSD@6.3kHz) with wave parameters. The results are divided into two groups according to the wind regimes (Figure 8a, upper panel). Circles represent increasing wind regime (I regime); diamonds represent decreasing wind regime (II regime). Dotted lines represent the best linear fit to I regime data; solid lines represent the best linear fit to II regime data. (For the interpretation of references to colour in this figure legend, the reader is referred to the web version of this article.)

Correlations between PSD and theoretical values of the total aerosol emissions have been calculated (Table 1). These correlations were calculated for the complete measurement time series and the two wind regimes defined earlier. For the function $F_{p14}(U_{10})$, the correlations, as expected, were high (0.92–0.95). For the wave state-dependent functions in the first regime of developing the wind wave conditions, the correlations were rather low (~0.42). In the second regime of the developed wind conditions, the correlations increased significantly (0.89 and 0.83).

The lower correlations between PSD and SSF in the developing wind conditions may be explained by the fact that the kinetic energy flux mostly came from the wind turbulence

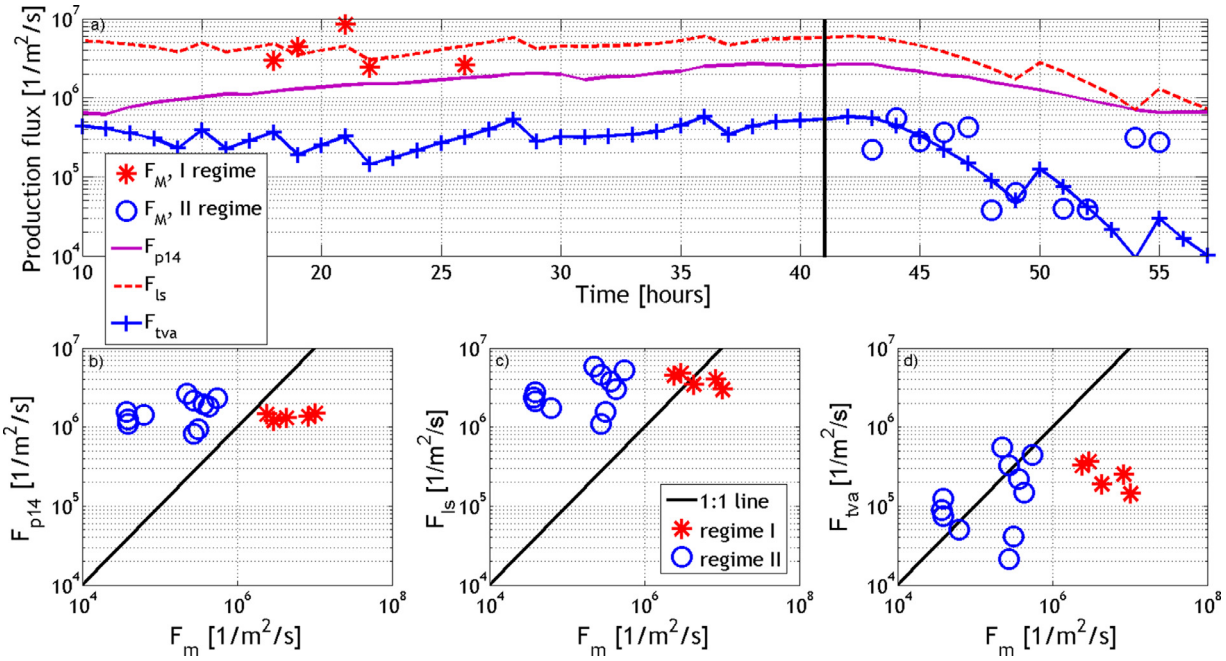

Figure 11 Comparison between the total measured production flux F_m and estimated SSF using sea spray generation functions: $F_{p14}(U_{10})$, $F_{ls}(H_s,\omega_p)$, $F_{tva}(H_s,\omega_p)$ (Eq. (1–3)). We can observe that in the first regime, the limiting steepness approach (ls, Eq. (2)) explains SSF better, while in the second regime the threshold vertical acceleration approach fits in better with the measured SSF.

Table 1 Correlation coefficients between measured Power Spectral Density (PSD) and theoretical total aerosol flux, estimated based on the three theoretical functions of Petelski et al. (2014): $F_{p14}(U_{10})$, Massel (2007) – $F_{ls}(H_s,\omega_p)$, and $F_{tva}(H_s,\omega_p)$. The total fluxes were obtained by integrating the aerosol size distribution within a range of particles D_p=(0.5, 47 μm).

	PSD@6.3 kHz		
	full time series	I regime	II regime
$F_{p14}(U_{10})$	0.92	0.95	0.94
$F_{ls}(H_s,\omega_p)$	0.71	0.39	0.89
$F_{tva}(H_s,\omega_p)$	0.69	0.42	0.83

to the wave field. So the primary factor which influenced the increase in SSF was wind speed. On the contrary, in the second period when waves were fully developed, the wind speed started decreasing, such that the SSF were more influenced by the inertia of the wave field and interference between waves. According to this, the two wave criteria of wave field description given by Massel (2007) predict quite well the two different physical phenomena of whitecaping, namely their impact on the SSF and noise of the bubbles.

During the developing wave state with increasing wind speed, there is generally an expected higher volume of air entrained to the water (Norris et al., 2013). The intensity of underwater noise caused by bubble bursting was higher as well (Figure 10). This phenomenon has to do with different energy dissipation mechanisms during both phases. That is why the increased population of bubbles influenced the total SSF by one order of magnitude higher in the first stage than in the second regime where the ambient noise was lower as well. This effect also influenced the SSF size distribution. As can be seen in Figure 8, the main difference in SSF was observed only for the submicron particles (D_p<2.5).

6. Conclusions

In this paper, we proposed and tested a method for predicting aerosol fluxes based on the underwater sound generated by local wind-dependent surface sources. The main objective of this study is to investigate the extent to which noise parameters can help estimate the aerosol sea spray source function, and our goal is to demonstrate the usefulness of using underwater sound recordings in monitoring local sources of aerosol generation.

Our attempt to ascertain these relations was motivated by the enormous progress in techniques, which allows underwater sea noise measurements to be performed for a long duration in a way that is affordable. Acoustic sensors deployed under the turbulent sea surface are durable and reliable. In contrast to the existing methods of aerosol flux measurements, the proposed method only needs a single receiver, in addition to relatively simple processing of only one-dimensional data. It would also seem promising to combine different methodologies from the various branches of marine sciences in the search for highly valuable results.

We presented an analysis of the relations between underwater noise and aerosol fluxes on the one hand, and different parameters of the wind wave field on the other. These new phenomena, explained by the limiting steepness and threshold vertical acceleration criteria, describe the SSF and bubbles noise behaviour fairly well. Compared with SSF

measurements, the generation function, based on the limiting steepness criterion, predicted the SSF in the case of the developing wave field much better. Based on the threshold vertical acceleration, the function was the best where it concerned agreement with the SSF for the developed wave field.

On that basis, the results of this study clearly indicate the possibility of being able to predict aerosol fluxes on account of underwater noise measurements. In other words, there is still the need for a more detailed inspection of wave field properties combined with bubble concentration monitoring. This study is further persuaded that for the latter to be accomplished, the focus ought to be on echo sounders anchored in areas with low-ship traffic.

Acknowledgments

This work was supported through a National Science Centre grant (BaSEAf: Baltic Sea European Arctic fluxes) id. number: 2015/17/N/ST10/02396.

We kindly thank the crew of the r/v *Oceania* for all technical assistance and safety care during the cruise. We thank two anonymous reviewers and editors of the journal for helpful comments and suggestions.

References

Abramowitz, M., Stegun, I.A., 1975. Handbook Of Mathematical Functions. Dover Publ., New York, 1045 pp.

Afeti, G.M., Resh, F.J., 1990. Distribution of the liquid aerosol produced from bursting bubbles in sea and distilled water. Tellus B 42, 378—384, https://doi.org/10.1034/j.1600-0889.1990.t01-2-00007.x.

Andreas, E.L., 2007. Comment on 'Vertical coarse aerosol fluxes in the atmospheric surface layer over the North Polar Water of the Atlantic' by Tomasz Petelski and Jacek Piskozub. J. Geophys. Res.-Oceans 112 (C11), art. C11010, https://doi.org/10.1029/2007JC004184.

Andreas, E.L., 1998. A New Sea Spray Generation Function for Wind Speeds up to 32 m/s. J. Phys. Oceanogr. 28, 2175—2184, https://doi.org/10.1175/1520-0485(1998)028⟨2175:ANSSGF⟩2.0.CO;2.

Andreas, E.L., 1992. Sea Spray and the Turbulent Air-Sea Heat Fluxes. J. Geophys. Res. 97, 11429—11441, https://doi.org/10.1029/92JC00876.

Andreas, E.L., 1995. The Temperature of Evaporating Sea Spray Droplets. J. Atmos. Sci. 52 (7), 852—862, https://doi.org/10.1175/1520-0469(1995)052⟨0852:TTOESS⟩2.0.CO;2.

Andreas, E.L., Jones, K.F., Fairall, C.W., 2010. Production velocity of sea spray droplets. J. Geophys. Res. 115, art. no. C12065, https://doi.org/10.1029/2010JC006458.

Blanchard, D.C., 1963. The electrification of the atmosphere by particles from bubbles in the sea. Prog. Oceanogr. 1, 73—112, https://doi.org/10.1016/0079-6611(63)90004-1.

Blanchard, D.C., 1964. Sea-to-Air Transport of Surface Active Material. Science 146 (3642), 396—397, https://doi.org/10.1126/SCIENCE.146.3642.396.

Blanchard, D.C., Syzdek, L.D., 1988. Film drop production as a function of bubble size. J. Geophys. Res. 93 (C4), 3649—3654, https://doi.org/10.1029/JC093iC04p03649.

Bortkovskii, R.S., Novak, V.A., 1993. Statistical dependencies of sea state characteristics on water temperature and wind-wave age. J. Mar. Syst. 4, 161—169, https://doi.org/10.1016/0924-7963(93)90006-8.

Bourassa, M.A., Vincent, D.G., Wood, W.L., Bourassa, M.A., Vincent, D.G., Wood, W.L., 2001. A Sea State Parameterization with Nonarbitrary Wave Age Applicable to Low and Moderate Wind Speeds. J. Phys. Oceanogr. 31, 2840—2851, https://doi.org/10.1175/1520-0485(2001)031⟨2840:ASSPWN⟩2.0.CO;2.

Callaghan, A.H., 2013. An improved whitecap timescale for sea spray aerosol production flux modeling using the discrete whitecap method. J. Geophys. Res. Atmos. 118 (17), 9997—10010, https://doi.org/10.1002/jgrd.50768.

Crouch, W.W., Burt, P.J., 1972. The Logarithmic Dependence of Surface-Generated Ambient-Sea-Noise Spectrum Level on Wind Speed. J. Acoust. Soc. Am. 51, 1066—1072, https://doi.org/10.1121/1.1912926.

de Leeuw, G., Andreas, E.L., Anguelova, M.D., Fairall, C.W., Lewis, E.R., O'Dowd, C., Schulz, M., Schwartz, S.E., 2011. Production flux of sea spray aerosol. Rev. Geophys 49 (2), art. no. 2010RG000349, https://doi.org/10.1029/2010RG000349.

de Leeuw, G., Neele, F.P., Hill, M., Smith, M.H., Vignati, E., 2000. Production of sea spray aerosol in the surf zone. J. Geophys. Res. Atmos. 105, 29397—29409, https://doi.org/10.1029/2000JD900549.

Deane, G.B., Stokes, M.D., 2002. Scale dependence of bubble creation mechanisms in breaking waves. Nature 418, 839—844, https://doi.org/10.1038/nature00967.

Dragan, A., Klusek, Z., Swerpel, B., 2011. Passive acoustic detection and observations of wind-wave breaking processes. Hydroacoustics 14, 29—38.

Esters, L., Landwehr, S., Sutherland, G., Bell, T.G., Christensen, K.H., Saltzman, E.S., Miller, S.D., Ward, B., 2017. Parameterizing air-sea gas transfer velocity with dissipation. J. Geophys. Res.-Oceans 122, 3041—3056, https://doi.org/10.1002/2016JC012088.

Fairall, C.W., Kepert, J.D., Holland, G.J., 1994. The effect of sea spray on surface energy transports over the ocean. Glob. Atmos. Ocean Syst. 2, 121—142.

Felizardo, F.C., Melville, W.K., Felizardo, F.C., Melville, W.K., 1995. Correlations between Ambient Noise and the Ocean Surface Wave Field. J. Phys. Oceanogr. 25, 513—532, https://doi.org/10.1175/1520-0485(1995)025⟨0513:CBANAT⟩2.0.CO;2.

Hasselmann, K., Barnett, T.P., Bouws, E., Carlson, H., Cartwright, D.E., Enke, K., Ewing, J.A., Gienapp, H., Hasselmann, D.E., Kruseman, P., Meerburg, A., Müller, P., Olbers, D.J., Richter, K., Sell, W., Walden, H., 1973. Measurements of wind-wave growth and swell decay during the Joint North Sea Wave Project (JONSWAP). Ergänzungsh, 8—12.

Hoppel, W.A., Frick, G.M., Fitzgerald, J.W., Larson, R.E., 1994. Marine boundary layer measurements of new particle formation and the effects nonprecipitating clouds have on aerosol size distribution. J. Geophys. Res. 99 (D7), 14443—14459, https://doi.org/10.1029/94JD00797.

IPCC — Intergovernmental Panel on Climate Change, 2013. Clouds and Aerosols. In: Climate Change 2013 — The Physical Science Basis: Working Group I Contribution to the Fifth Assessment Report of the Intergovernmental Panel on Climate Change. Cambridge Univ. Press, Cambridge, 571—657.

Jensen, D.R., Gathman, S.G., Zeisse, C.R., McGrath, C.P., De Leeuw, G., Smith, M.A., Frederickson, P.A., Davidson, K.L., 2001. Electro-optical propagation assessment in coastal environments (EOPACE): summary and accomplishments. Opt. Eng. 40 (8), 13 pp., https://doi.org/10.1117/1.1387985.

Kerman, B.R., 1984. Underwater sound generation by breaking wind waves. J. Acoust. Soc. Am. 75, 149—165, https://doi.org/10.1121/1.390409.

Kiger, K.T., Duncan, J.H., 2012. Air-Entrainment Mechanisms in Plunging Jets and Breaking Waves. Annu. Rev. Fluid Mech. 44, 563—596, https://doi.org/10.1146/annurev-fluid-122109-160724.

Klusek, Z., 2011. Ambient sea noise in the Baltic Sea — review of investigations. Hydroacoustics 14, 75—82.

Klusek, Z., Lisimenka, A. , 2016. Seasonal and diel variability of the underwater noise in the Baltic Sea. J. Acoust. Soc. Am, 139, art. no. 1537, https://doi.org/10.1121/1.4944875.

Koga, M., 1981. Direct production of droplets from breaking wind-waves its observation by a multi-colored overlapping exposure photographing technique. Tellus 33, 552—563, https://doi.org/10.1111/j.2153-3490.1981.tb01781.x.

Komen, G.J., 1994. Dynamics and modelling of ocean waves. Cambridge Univ. Press, Cambridge, 532 pp.

Kraan, G., Oost, W.A., Janssen, P.A.E.M., 1996. Wave Energy Dissipation by Whitecaps. J. Atmos. Ocean. Technol. 13, 262—267, https://doi.org/10.1175/1520-0426(1996)013⟨0262:WEDBW⟩2.0.CO;2.

Lewis, E.R., Schwartz, S.E. , 2004. Sea salt aerosol production: Mechanisms, methods, measurements and models — A critical review. Geophys. Monogr. Ser, 152, 413 pp, https://doi.org/10.1029/152GM01.

Lhuissier, H., Villermaux, E., 2012. Bursting bubble aerosols. J. Fluid Mech. 696, 5—44, https://doi.org/10.1017/jfm.2011.418.

Loewen, M.R., Melville, W.K., 1991. Microwave backscatter and acoustic radiation from breaking waves. J. Fluid Mech. 224, 601—623, https://doi.org/10.1017/S0022112091001891.

MacIntyre, F., 1972. Flow patterns in breaking bubbles. J. Geophys. Res. 77, 5211—5228, https://doi.org/10.1029/JC077i027p05211.

Marks, R., 1990. Preliminary investigations on the influence of rain on the production, concentration, and vertical distribution of sea salt aerosol. J. Geophys. Res. 95 (C12), 22299—22304, https://doi.org/10.1029/JC095iC12p22299.

Markuszewski, P., Kosecki, S., Petelski, T., 2017a. Sea spray aerosol fluxes in the Baltic Sea region: Comparison of the WAM model with measurements. Estuar. Coast. Shelf Sci. 195, 16—22, https://doi.org/10.1016/j.ecss.2016.10.007.

Markuszewski, P., Rozwadowska, A., Cisek, M., Makuch, P., Petelski, T., 2017b. Aerosol physical properties in Spitsbergen's fjords: Hornsund and Kongsfjorden during AREX campaigns in 2014 and 2015. Oceanologia 59 (4), 460—472, https://doi.org/10.1016/J.OCEANO.2017.03.012.

Massel, S.R., 2007. Ocean Waves Breaking and Marine Aerosol Fluxes. Atmos. Ocenaogr. Sci. Library, 38. Springer-Verlag, New York, 316 pp., https://doi.org/10.1007/978-0-387-69092-6.

Massel, S.R., 2018. Ocean surface waves: Their physics and prediction. Adv. Ser. Ocean Eng., World Sci., 800 pp., https://doi.org/10.1142/10666.

Medwin, H., Beaky, M.M., 1989. Bubble sources of the Knudsen sea noise spectra. J. Acoust. Soc. Am. 86 (3), 1124—1130, https://doi.org/10.1121/1.398104.

Minnaert, M., 1933. XVI. *On musical air-bubbles and the sounds of running water*. London, Edinburgh. Dublin Philos. Mag. J. Sci. 16 (104), 235—248, https://doi.org/10.1080/14786443309462277.

Monahan, E.C., Fairall, C.W., Davidson, K.L., Boyle, P.J., 1983. Observed inter-relations between 10 m winds, ocean whitecaps and marine aerosols. Q. J. R. Meteorol. Soc. 109, 379—392, https://doi.org/10.1002/qj.49710946010.

Monin, A.S., Obukhov, A.M., 1954. Basic laws of turbulent mixing in the surface layer of the atmosphere. Tr. Akad. Nauk SSSR Geophiz. Inst. 24 (151), 163—187.

Norris, S.J., Brooks, I.M., Hill, M.K., Brooks, B.J., Smith, M.H., Sproson, D.A.J., 2012. Eddy covariance measurements of the sea spray aerosol flux over the open ocean. J. Geophys. Res. 117 (D7), art. no. D07210, https://doi.org/10.1029/2011JD016549.

Norris, S.J., Brooks, I.M., Moat, B.I., Yelland, M.J., de Leeuw, G., Pascal, R.W., Brooks, B., 2013. Near-surface measurements of sea spray aerosol production over whitecaps in the open ocean. Ocean Sci 9, 133—145, https://doi.org/10.5194/os-9-133-2013.

Nystuen, J.A., 2001. Listening to raindrops from underwater: An acoustic disdrometer. J. Atmos. Ocean. Technol. 18 (10), 1640—1657, https://doi.org/10.1175/1520-0426(2001)018⟨1640:LTRFUA⟩2.0.CO;2.

Petelski, T., 2005. Coarse Aerosol Concentration Over the North Polar Waters of the Atlantic. Aerosol Sci. Technol. 39, 695—700, https://doi.org/10.1080/02786820500182362.

Petelski, T., 2003. Marine aerosol fluxes over open sea calculated from vertical concentration gradients. J. Aerosol Sci. 34, 359—371, https://doi.org/10.1016/S0021-8502(02)00189-1.

Petelski, T., Markuszewski, P., Makuch, P., Jankowski, A., Rozwadowska, A., 2014. Studies of vertical coarse aerosol fluxes in the boundary layer over the Baltic Sea. Oceanologia 56 (4), 697—710, https://doi.org/10.5697/oc.56-4.697.

Petelski, T., Piskozub, J. , 2006. Vertical coarse aerosol fluxes in the atmospheric surface layer over the North Polar Waters of the Atlantic. J. Geophys. Res, 111 (C6), art. no. C06039, https://doi.org/10.1029/2005JC003295.

Petelski, T., Piskozub, J., Paplińska-Swerpel, B., 2005. Sea spray emission from the surface of the open Baltic Sea. J. Geophys. Res.-Oceans, 110 (C10), art. no. C10023, https://doi.org/10.1029/2004JC002800.

Prosperetti, A., 1988. Bubble-related ambient noise in the ocean. J. Acoust. Soc. Am. 84, 1042—1054, https://doi.org/10.1121/1.396740.

Prosperetti, A., Lu, N.Q., Kim, H.S., 1993. Active and passive acoustic behavior of bubble clouds at the ocean's surface. J. Acoust. Soc. Am. 93, 3117—3127, https://doi.org/10.1121/1.405696.

Resch, F.J., Darrozes, J.S., Afeti, G.M., 1986. Marine liquid aerosol production from bursting of air bubbles. J. Geophys. Res. 91 (C1), 1019—1029, https://doi.org/10.1029/JC091iC01p01019.

Savelyev, I.B., Anguelova, M.D., Frick, G.M., Dowgiallo, D.J., Hwang, P.A., Caffrey, P.F., Bobak, J.P., 2014. On direct passive microwave remote sensing of sea spray aerosol production. Atmos. Chem. Phys. 14, 11611—11631, https://doi.org/10.5194/acp-14-11611-2014.

Sellegri, K., O'Dowd, C.D., Yoon, Y.J., Jennings, S.G., de Leeuw, G., 2006. Surfactants and submicron sea spray generation. J. Geophys. Res. 111, art. no. D22215, https://doi.org/10.1029/2005JD006658.

Smith, M.H., Park, P.M., Consterdine, I.E., 1993. Marine aerosol concentrations and estimated fluxes over the sea. Q. J. R. Meteorol. Soc. 119, 809—824, https://doi.org/10.1002/qj.49711951211.

Spiel, D.E., 1998. On the births of film drops from bubbles bursting on seawater surfaces. J. Geophys. Res.-Oceans 103, 24907—24918, https://doi.org/10.1029/98JC02233.

Stramska, M., Petelski, T., 2003. Observations of oceanic whitecaps in the north polar waters of the Atlantic. J. Geophys. Res. 108 (C3), 108 (C3), art. no. 3086, https://doi.org/10.1029/2002JC001321.

Tsigaridis, K., Koch, D., Menon, S., 2013. Uncertainties and importance of sea spray composition on aerosol direct and indirect effects. J. Geophys. Res. Atmos. 118, 220—235, https://doi.org/10.1029/2012JD018165.

Vagle, S., Large, W.G., Farmer, D.M., Vagle, S., Large, W.G., Farmer, D.M., 1990. An Evaluation of the WOTAN Technique of Inferring Oceanic Winds from Underwater Ambient Sound. J. Atmos. Ocean. Technol. 7, 576—595, https://doi.org/10.1175/1520-0426(1990)007⟨0576:AEOTWT⟩2.0.CO;2.

Vakkayil, R., Graber, H.C., Large, W.G., 1996. Oceanic winds estimated from underwater ambient noise observations in SWADE. In: OCEANS 96 MTS/IEEE Conf. Proc. The Coastal Ocean — Prospects for the 21st Century. IEEE, 45—51.

Veron, F., 2015. Ocean Spray. Ann. Rev. Fluid Mech. 47, 507—538, https://doi.org/10.1146/annurev-fluid-010814-014651.

WAMDI Group, 1988. The WAM Model. J. Phys. Oceanogr. 18, 1775—1810 , https://doi.org/10.1175/1520-0485(1988)018<1775:TWMTGO>2.0.CO;2.

Wenz, G.M., 1962. Acoustic Ambient Noise in the Ocean: Spectra and Sources. J. Acoust. Soc. Am. 34, 1936—1956, https://doi.org/10.1121/1.1909155.

Wilson, J.D., Makris, N.C., 2008. Quantifying hurricane destructive power, wind speed, and air-sea material exchange with natural undersea sound. Geophys. Res. Lett 35 (10), art. no. L10603, https://doi.org/10.1029/2008GL033200.

Wilson, P.R., 1980. The interaction of acoustic waves with flux tubes. Astrophys. J. 237, 1008—1014, https://doi.org/10.1086/157946.

Wu, J., 2002. Jet Drops Produced by Bubbles Bursting at the Surface of Seawater. J. Phys. Oceanogr. 32, 3286—3290, https://doi.org/10.1175/1520-0485(2002)032⟨3286:JDPBBB⟩2.0.CO;2.

Wu, J., 1993. Production of spume drops by the wind tearing of wave crests: The search for quantification. J. Geophys. Res. 98 (C10), 18221—18227, https://doi.org/10.1029/93JC01834.

Wu, J., 1981. Evidence of Sea Spray Produced by Bursting Bubbles Science, 212, 324—326.

Zedel, L., Gordon, L., Osterhus, S., Zedel, L., Gordon, L., Osterhus, S., 1999. Ocean Ambient Sound Instrument System: Acoustic Estimation of Wind Speed and Direction from a Subsurface Package. J. Atmos. Ocean. Technol. 16, 1118—1126, https://doi.org/10.1175/1520-0426(1999)016⟨1118:OASISA⟩2.0.CO;2.